9B.5   **RADAR OBSERVATIONS OF TURBULENCE AND WIND SHEAR**

Valery M. Melnikov CIMMS/University of Oklahoma,
Richard J. Doviak; National Severe Storms Laboratory/NOAA and
Ming Fang CIMMS/University of Oklahoma

Introduction

Radar observations in widespread precipitation often reveal layers of enhanced spectrum widths. A vertical radar cross section (RHI) of a spectrum width field is shown in Fig. 1, wherein one can see a layer of large widths at the height of about 2.5 .. 3 km. In this layer, maximal spectrum widths reach 13 m s^{-1}; this is well above the medium spectrum width values found in thunderstorms and squall lines (i.e., up to 6 m s^{-1}; Fang and Doviak, 2001). Layers of spectrum widths of more than 6 m s^{-1} are not rare in Oklahoma. The spectrum widths in the layer in Fig. 1 become less at closer ranges. This suggests that the dominant process of spectrum broadening is vertical shear of the horizontal wind. That is, at closer ranges the antenna beam becomes narrower making the wind shear contribution smaller, and the angle between the horizontal wind and the antenna increases driving the shear contribution further down. Disappearance of the layer at close ranges allows us to conclude that there is no significant turbulence in the layer. But this deduction implies that the layer has horizontally homogeneous characteristics.
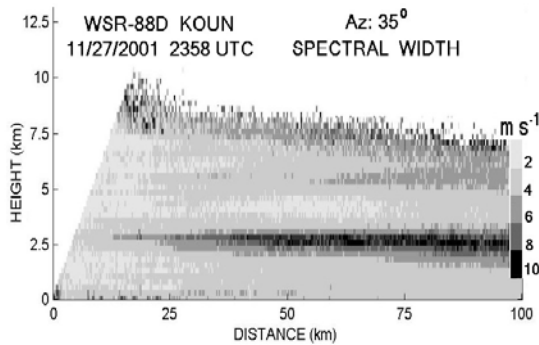

Fig. 1.   Vertical cross section of widespread precipitation on Nov. 27, 2001

Corresponding author's address:
Valery.Melnikov@noaa.gov

The spectrum width, σ_v, of Doppler spectra has contributions from turbulence, radial wind shear, fall speeds of the droplets, droplets' oscillations, and antenna rotation. For radar observations with the WSR-88D, radial wind shear, often due to strong uniform wind blowing across the beam, and turbulence contributions are much larger than the other causes (Doviak and Zrnic, 1993, Section 5.3). So the spectrum width can be written in a form,

$$\sigma_v^2 = \sigma_{v\,tur}^2 + \sigma_{v\,sr}^2 + \sigma_{v\,sa}^2 + \sigma_{v\,se}^2, \quad (1)$$

where the first term on the right side of (1) is the turbulent contribution and the three others are wind shear contributions for radial (sr), azimuthal (sa), and elevation (se) directions. Istok and Doviak (1986) came to a conclusion that in thunderstorms, the spectrum broadening is primarily due to turbulence. In stratiform precipitation, Doppler velocity fields have more simple patterns than in thunderstorms. Despite this, there have been few attempts (e.g., Fang, 2003) to separate turbulence and wind shears in stratiform weather having regions of extremely large spectrum widths. We present here some results for widespread precipitation with zones of spectrum width larger than 5 m s^{-1}. Radar cross sections presented here have been recorded with NSSL's Research & Development WSR-88D.

Turbulent and wind shear contributions to the spectrum width

The wind shear contributions to the spectrum width can be calculated from measured Doppler velocities. The radial wind shear contributions in (1) can be written in a form (Doviak, Zrnic, 1993, section 5.3):

$$\sigma_{v\,sr} = 0.175 c\tau k_r,$$

$$\sigma_{v\,sa} = \sigma_\theta r k_\varphi, \qquad \qquad (2)$$

$$\sigma_{v\,se} = \sigma_\theta r k_e$$

where $\sigma_\theta = \theta_1 /(4 \ln^{1/2} 2)$, θ_1 is the one-way 3-dB antenna beamwidth, which is considered to be equal in azimuthal and elevation directions, r is the distance to the radar volume, c is speed of light, τ is the radar pulse duration, k_φ, k_e and k_r are the Doppler velocity shears in azimuthal, elevation, and radial directions. The formula to compute spectrum width due to shear in the radial direction assumes that the radar's receiver's bandwidth is large compared to the reciprocal of the pulse width. The first term in (2) can be computed easily from Doppler velocities for two adjacent range gates in a given radial of data. The azimuth shear can be calculated from the velocity field in a slant radar cut (i.e., from a PPI scan) using the Doppler velocities from two adjacent radials at the same range. The elevation shear can be obtained from Doppler velocities on two consecutive PPIs at different elevation angles. Istok and Doviak (1986) calculated the azimuthal and elevation shears using the nine-point least-square approximation of the Doppler velocities for three consecutive PPIs at different elevation angles. The data was collected during Doppler radar observations with elevation increment of 1^0. For thin vertical layers of wind shears like in Fig. 1, this increment can be too big.

To obtain the wind shear in a thin vertical layer, the radar data with fine elevation resolution is needed. Thus vertical cross sections (RHIs) are more appropriate for such measurements. To conduct a detailed analysis of the wind shear contributions, we collected the radar data making RHIs with a fine elevation resolution of 0.125^o. The RHIs allow obtaining the elevation and radial shears. To calculate the azimuthal wind shear, we made two or three consecutive RHIs with an azimuthal stride of 2^0. Current configuration of our processing system allows making two such RHIs during a time interval of 2 min. So we assume that the Doppler velocity and spectrum width fields do not change significantly during the period of 2 min. Indeed, the layer patterns like in Fig. 1 are observed much longer. To reduce statistical uncertainties of spectrum width measurements, 256 sample records are used for estimation of the radar moments.

The azimuthal, elevation, and radial wind shear contributions were calculated as follows. Using two RHIs, say A and B, the azimuthal shear for a given radial m and given resolution volume n, is $k_\theta(A, m, n) = [v(A, m, n) - v(B, m, n)]/\Delta\varphi$, where $v(A, m, n)$ is the measured Doppler velocity and $\Delta\varphi$ is the azimuth separation of the RHIs A and B. In our measurements, $\Delta\varphi = 2^o$. The elevation shear is calculated as $k_e(A, m, n) = [v(A, m-1, n) - v(A, m+1, n)]/2\Delta\theta$, where $\Delta\theta$ is the elevation step; in our measurements, $\Delta\theta = 0.125^o$. The radial shear is obtained as $k_r(A, m, n) = [v(A, m, n+1) - v(A, m, n)]/\Delta r$, where Δr is the resolution volume spacing in range; in our measurements, $\Delta r = 250$ m. The total shear and turbulent contributions were calculated using Eqs. (2) and (1).

In Fig. 2, Doppler velocity and spectrum width data vs elevation angle at a 40 km range are shown for the cross section presented in Fig.1. This figure also presents the calculated profiles of wind shear and turbulence contributions to σ_v. The turbulence contribution is obtained by subtracting the sum of spectrum variances due to shear from the measured spectrum width squared. The azimuthal shear contribution profile is not shown because it was about two orders of magnitude less than the elevation shear contribution. One can see that in the region of enhanced spectrum width, the elevation shear contribution is very close to the measured spectrum width, i.e., the main contributor to the spectrum width is from the vertical shear of the horizontal wind.
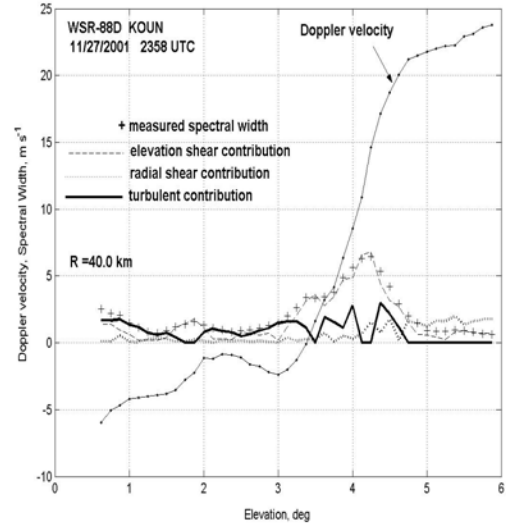

Fig. 2. Elevation dependence of measured Doppler velocities and spectrum widths and calculated turbulent, radial shear and elevation shear contributions using data in Fig. 1 from the range of 40 km.

Having obtained the wind shear and turbulent contributions to the spectrum width,
the turbulent dissipation rate can be calculated using the following equations (Doviak and Zrnic 1993, section 10.3):

$$\sigma^3_{v\,tur} = 1.39 A^{3/2} \varepsilon \sigma_\theta r, \qquad \sigma_\theta r > \Delta r ,$$

$$\sigma^3_{v\,tur} = (1.35 A)^{3/2} \varepsilon \Delta r \chi^{3/2}, \quad \sigma_\theta r \le \Delta r ,$$

$$\chi = 11/15 + (4/15) r^2 \sigma^2_\theta / \Delta r^2, \qquad (3)$$

where A is the universal dimensionless constant, we used $A = 1.55$.

Fig. 3 presents the turbulence contribution to the spectrum width for the cross section in Fig. 1. One can see that enhanced turbulence is in three layers: the strongest is at the center of the layer of strong widths at 2.5 km. A second broad layer is at the heights between 0 to 2 km, and a third layer is at the top of the clouds between 6 and 8 km. In the layers, the turbulent dissipation rates calculated using (3) are as follows. In the first layer (i.e., at 2.5 km), maximal value of the eddy dissipation rate reaches 0.03 m^2s^{-3} , suggesting moderate to severe turbulence (Doviak and Zrnic, 1993, Fig. 11.18). The mean value of the turbulent dissipation rate in the second layer is 0.003 m^2s^{-3} with a maximal value of about 0.01 m^2s^{-3}, corresponding to light to moderate turbulence. In the top layer, the mean dissipation rate is between 0.007 and 0.008 m^2s^{-3}.

In the layer of large spectrum widths in Fig. 1, the azimuthal shears were less than 7 10^{-4} s^{-1} with the mean value of 2 10^{-4} s^{-1}; the vertical shear of horizontal wind shear reaches 5.1 10^{-2} s^{-1} with the mean value near 2.5 10^{-2} s^{-1}.

We have analyzed several cases with layers of large spectrum width as in Fig. 1 and found that if the vertical shear is smaller than 2 10^{-2} s^{-1}, there are no significant turbulent contributions. For higher wind shears, in layers of large spectrum widths, there remains a thin layer of turbulence like in Fig. 3. There could be an effect of smoothing with antenna's radiation pattern which can underestimate strong elevation shears and correspondingly overestimate turbulent contributions.
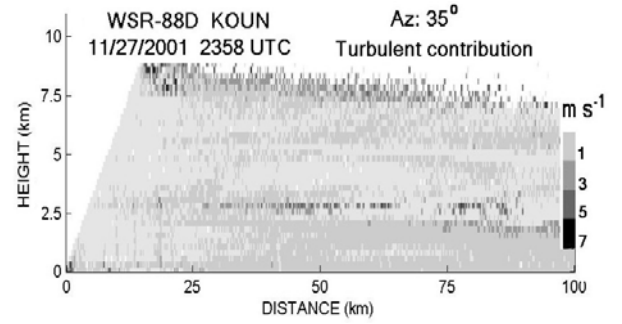

Fig. 3. Turbulent contribution to spectrum widths in Fig. 1.

Spectrum width patterns in widespread precipitation

Our radar observations of spectrum width in widespread precipitation reveal variety of field patterns. In vertical cross sections, we often observe layers of enhanced spectrum widths like in Fig. 1. Sometimes, layers of enhanced widths have wavy patterns. In Fig. 4 one can see such a pattern at the heights near 6 km at distances of 25 to 40 km.

Fig. 5 shows a pattern in a form of a "cat's eye" (Gossard and Hooke, 1975) that can be seen at heights of 3.5 to 5 km at the distances of 50 to 80 km. One can see a pattern with nearly closed almost circular structures. Fig. 6 represents a patchy pattern of spectrum width field. Fig. 7 shows the turbulent contribution to the spectrum widths obtained with the techniques described in previous section. One can see definite periodicity in turbulent patches.

Often, spectrum width fields show patterns more clearly than corresponding patterns in Doppler velocity fields. We stress ones more that the patterns presented here are collected on the WSR-88D radar with small elevation step of 0.125^0. These structures can not be revealed from standard WSR-88D observations because the 1^0 standard elevation increments are too large.
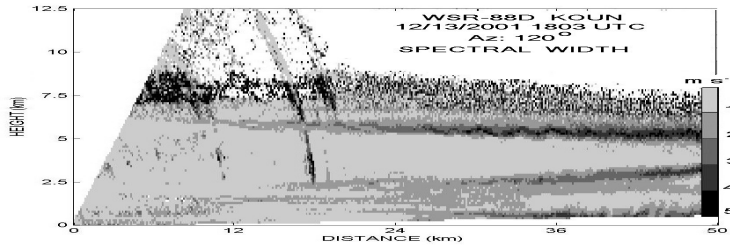
Fig. 4. Stratiform precipitation on Dec.13, 2001. Note a wavy layer at height of 6 km.
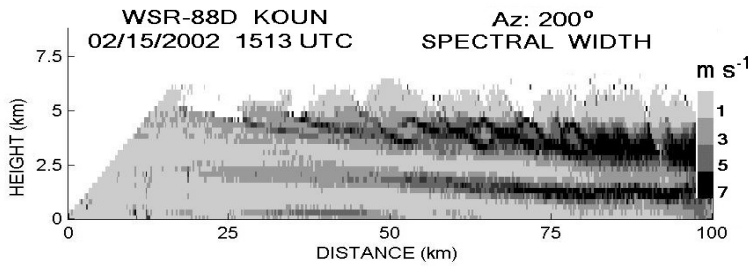

Fig. 5. Spectrum width pattern in a form of "cat's eye" structures at heights of 4 to 5 km at ranges of 50 to 80 km
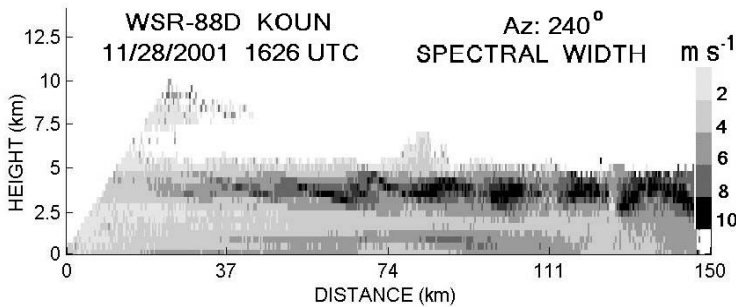

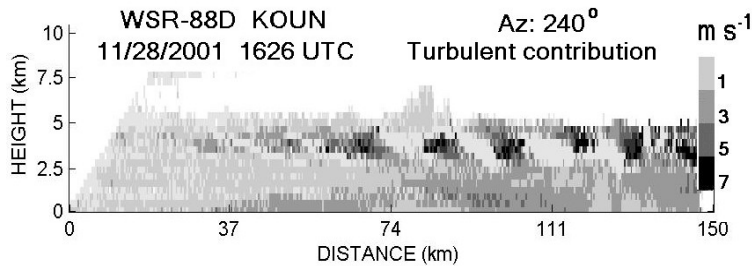Fig. 6. Spectrum width pattern in a form of patches.

Fig 7. Turbulent contribution to the spectrum width field shown in Fig. 6.

References

Doviak, R. J., and D. S. Zrnic, 1993: *Doppler radar and weather observations*, 2nd ed., Academic Press, 562 pp.

Fang, M., 2003. Spectrum width statistics of various weather phenomena and comparison of observations with simulations. MS thesis, University of Oklahoma.

Fang, M., and R. J. Doviak, 2001: Relating WSR-88D spectrum width data to various weather conditions. 30th International Conference on Radar Meteorology, Amer. Meteor. Soc., Boston, MA., 382-384.

Gossard, E. E., and Hooke, W. H. 1975: *Waves in the Atmosphere: Atmospheric Infrasound and Gravity Waves-Their Generation and Propagation.* Elsevier, Amsterdam, 456 pp.

Istok, M. J., and Doviak R. J., 1986: Analysis of the relation between Doppler spectra width and thunderstorm turbulence. *J. Atmos .Sci.*, **48,** 2199-2214.